Early mandibular morphological differences in patients with FGFR2 and FGFR3-related syndromic craniosynostoses: a 3D comparative study

A. Morice, Raphael Cornette, A. Giudice, C.D. Collet, G. Paternoster, Éric Arnaud, E. Galliani, A. Picard, L. Legeai-Mallet, R.H. Khonsari

Title page

Early mandibular morphological differences in patients with *FGFR2* and *FGFR*3-related syndromic craniosynostoses: a 3D comparative study

MORICE A., MD[1,2], CORNETTE R., PhD[3], GIUDICE A., MD, PhD[4], COLLET C., D.Pharm PhD[5,6], PATERNOSTER G., MD[7], ARNAUD É., MD[7], GALLIANI E., MD[1], PICARD A., MD, PhD[1], LEGEAI-MALLET L., PhD[2], KHONSARI R.H., MD, PhD[1,2,7]

1. Service de chirurgie maxillo-faciale et chirurgie plastique, Hôpital Universitaire Necker – Enfants Malades, Assistance Publique – Hôpitaux de Paris ; Centre de Référence Maladies Rares MAFACE Fentes et Malformations Faciales ; Université de Paris ; Paris, France
2. Laboratoire 'Bases Moléculaires et Physiopathologiques des Ostéochondrodysplasies', INSERM UMR 1163, Institut Imagine, Paris, France.
3. Institut de Systématique, Evolution, Biodiversité (ISYEB), Muséum national d'Histoire naturelle, Sorbonne Université, Ecole Pratique des Hautes Etudes, Université des Antilles, CNRS ; CP 50, 57 rue Cuvier 75005 Paris, France.
4. Università degli Studi di Catanzaro 'Magna Graecia', Catanzaro, Italy
5. BIOSCAR, INSERM U1132, Université de Paris, Hôpital Lariboisière, 75010 Paris
6. Service de Biochimie et Biologie Moléculaire, CHU-Paris-GH Saint Louis Lariboisière Widal, Paris, France.
7. Service de neurochirurgie, Hôpital Universitaire Necker – Enfants Malades, Assistance Publique – Hôpitaux de Paris ; Centre de Référence Maladies Rares CRANIOST Cranioténoses et Malformations Craniofaciales ; Université de Paris ; Paris, France

Corresponding author:
Anne Morice
Service de chirurgie maxillo-faciale et chirurgie plastique
Hôpital Necker - Enfants Malades
149 rue de Sèvres
75015 Paris
email: annemoriceaertgeerts@gmail.com

Declarations of interest: none

Word count:
Abstract: 304
Manuscript: 3661

Abstract

Syndromic craniosynostoses are defined by the premature fusion of one or more cranial and facial sutures, leading to skull vault deformation, and midfacial retrusion. More recently, mandibular shape modifications have been described in *FGFR*-related craniosynostoses, which represent almost 75 % of the syndromic craniosynostoses. Here, further characterisation of the mandibular phenotype in *FGFR*-related craniosynostoses is provided in order to confirm mandibular shape modifications, as this could contribute to a better understanding of the involvement of the FGFR pathway in craniofacial development.

The aim of our study was to analyse early mandibular morphology in a cohort of patients with *FGFR2*- (Crouzon and Apert) and *FGFR3*- (Muenke and Crouzonodermoskeletal) related syndromic craniosynostoses. We used a comparative geometric morphometric approach based on 3D imaging. Thirty-one anatomical landmarks and eleven curves with sliding semi-landmarks were defined to model the shape of the mandible.

In total, 40 patients (12 with Crouzon, 12 with Apert, 12 with Muenke and 4 with Crouzonodermoskeletal syndromes) and 40 age and sex-matched controls were included (mean age: 13.7 months ± 11.9). Mandibular shape differed significantly between controls and each patient group based on geometric morphometrics. Mandibular shape in *FGFR2*-craniosynostoses was characterized by open gonial angle, short ramus height, and high and prominent symphysis. Short ramus height appeared more pronounced in Apert than in Crouzon syndrome. Additionally, narrow inter-condylar and inter-gonial distances were observed in Crouzon syndrome. Mandibular shape in *FGFR3*-craniosynostoses was characterized by high and prominent symphysis and narrow inter-gonial distance. In addition, narrow condylar processes affected patients with Crouzonodermoskeletal syndrome.

Statistical analysis of variance showed significant clustering of Apert and Crouzon, Crouzon and Muenke, and Apert and Muenke patients ($p<0.05$).

Our results confirm distinct mandibular shapes at early ages in *FGFR2*- (Crouzon and Apert syndromes) and *FGFR3*-related syndromic craniosynostoses (Muenke and Crouzonodermoskeletal syndromes) and reinforce the hypothesis of genotype-phenotype correspondence concerning mandibular morphology.

Keywords

Craniosynostosis; FGFR2; FGFR3; mandibular shape; 3D geometric morphometrics

Introduction

Craniosynostoses – reported in 1:2,000 to 1:3,000 live births, comprising at least 20 % of syndromic cases [1] – are defined by the premature fusion of one or more cranial and facial sutures, leading to various craniofacial anomalies, among which: skull vault deformation, potentially causing increased intracranial pressure, shallow orbits leading to exorbitism, and midfacial retrusion that can be associated with obstructive sleep apnoea syndrome [2-4].

Various mutations have been reported in syndromic craniosynostoses and affect key signalling pathways involved in craniofacial development, such as FGFRs/TWIST pathways, MSX2, EFR, TCF12 and SMAD6 [5]. Mutations in genes from the FGFR (Fibroblast Growth Factor Receptor) pathways are reported in almost 75% of syndromic craniosynostoses [6]. Such *FGFR*-related conditions are due to specific activating heterozygous mutations localized in *FGFR1* (Pfeiffer syndrome type 1) [1], *FGFR2* (Apert, Crouzon, Pfeiffer type 2 and 3 syndromes, Antley-Bixler, Beare-Stevenson cutis gyrata syndromes, Bent Bone Dysplasia and Saethre-Chotzen like syndrome) [5-9] and *FGFR3* genes (Muenke syndrome and Crouzonodermoskeletal syndrome). Muenke syndrome is the most frequent *FGFR*-related syndromic craniosynostosis [10]. Crouzonodermoskeletal syndrome is an exceedingly rare syndrome sharing similarities with Crouzon syndrome and including skin lesions (*acanthosis nigricans*) [11-14]. Most of these FGFR mutations are gain of function, inducing high activity of the receptor in presence and in absence of its FGF ligands, thus disturbing bone formation.

It has been demonstrated that *FGFR* genes are implicated in bone formation and both axial and appendicular skeletal development as illustrated by the phenotype of chondrodysplasia [15-18]. Skull vault, frontal bone and midfacial anomalies have been extensively described in *FGFR*-related syndromic craniosynostoses [3,19-22]. Several studies also report mandibular

115 shape modifications in *FGFR2*- and *FGFR3*-related craniosynostoses [23-27] as well as in
116 achondroplasia (*FGFR3*) [28].
117 The mandible is a dermal bone derived from neural crest cells migrating into the first
118 pharyngeal arch [29-33]. Mandibular bone ossifies early during the 6th week of pregnancy
119 [34]. In mouse and chick models, *Fgfr2* and *Fgfr3* genes are expressed during mandibular
120 formation at the sites of primary (Meckel cartilage) and secondary cartilages (condyles,
121 symphysis) and have key roles in mandibular intramembranous and endochondral ossification
122 [35-39].
123 A better characterisation of the human mandibular phenotype is necessary in *FGFR*-related
124 craniosynostoses. This could help to better understand the implication of the FGFR pathway
125 in craniofacial development and highlight homologies between mouse models and human
126 phenotypes.
127 The aim of our study was to analyse mandibular morphology at early ages in a cohort of
128 patients with *FGFR2*- (Crouzon and Apert) and *FGFR3*- (Muenke and
129 Crouzonodermoskeletal) related syndromic craniosynostoses, using a comparative geometric
130 morphometric approach based on 3D imaging, allowing shape comparisons between each
131 *FGFR*-craniosynostosis subtype and age and sex-matched controls, and between the different
132 *FGFR*-craniosynostosis subtypes.
133
134
135
136
137
138
139

Patients and methods

Patients

We retrospectively included 40 patients presenting with genetically confirmed *FGFR2*- or *FGFR3*-related syndromic craniosynostoses, and available craniofacial computed tomographic (CT) scan. Only CT-scans performed at early ages before fronto-facial or fronto-orbital advancement, or in the immediate post-operative period after posterior vault expansion (at post-operative days 1 or 2), were included, in order to avoid potential confounding factors related to the effects of surgery on mandibular shape. The following clinical parameters were collected: gender, type of mutation, age at CT-scan and at first surgical procedure and tracheostomy. The database used to select patients covered the birth period 2003-2017. All patients were initially managed in the National Referral Center for craniofacial malformations (Centre de Référence Maladies Rares CRANIOST), located within our hospital. The study was approved by the local Ethical Committee (Comité d'Éthique de Necker – Enfants Malades, approval number: 2018 RK18).

Controls

Controls were selected among age and gender-matched patients free of any reported craniofacial anomalies who underwent CT-scans for the assessment of benign craniofacial trauma or infections (mandible excluded). All CT-scans were extracted from the same database (clinical database of Necker – Enfants Malades).

Comparative study of mandibular morphology based on 3D geometric morphometrics

Segmentation and 3D reconstructions were performed based on DICOM raw data using 3D Slicer 4 [40] by isolating the mandible based on its cortical and trabecular bone density thresholds. Visual adjustments of the cortical bone density threshold were done for each CT-scan, without smoothing factors to keep the correct contours and avoid any loss of information concerning anatomical variations. The 3D surface mesh obtained for each patient and control was saved in STL format.

Thirty-one anatomical landmarks and eleven curve with sliding semi-landmarks were defined in order to model the shape of the mandible, based on previous studies [41-43] and were placed using Viewbox 4 (dHal Software, Kifissia, Greece), by the same author (AM). Names and definitions of the landmarks and curves are provided on Figure 1. Using Morpho J v. 1.06 [44], a Procrustes ANOVA analysis for error measurement of 'factor repetition' showed no significant differences in landmarking positioning, allowing valid comparative analysis of shape variability among individuals (see Supplementary Table 1).

Comparative mandibular morphology was assessed based on 3D geometric morphometrics [45] using R [46] for data processing. Landmarks coordinates were superimposed using a Generalized Procrustes Analysis (GPA) [47]. Sliding semi-landmarks of curves have been allowed to slide minimizing the bending energy [43] using the 'gpagen' function of the 'geomorph' package [48]. Coordinates after GPA were assessed using principal component analysis (PCA) which gives information about raw variability. Both analyses, GPA and PCA were performed using the 'gpagen' and 'plotTangentSpace' functions of the 'geomorph' package [48]. Ten PC axis have been kept for statistical analysis representing 90 % of total shape variation [49]. The 3D visualizations along the axes of the PCA have been made using 'Thin Plate Splines' (TPS) [50], from the average shape to the extremes shapes of the axes thanks to the 'tps3d' function of the 'Morpho' package [50]. In a first step, the 3D model of a

control specimen (representative of the median age of the studied population) has been warped to the mean shape (corresponding to the mean coordinates of all specimens, defining the area 'zero' of the PCA) to create a 3D model of the mean shape. In a second step, this 3D mean shape has been deformed using TPS interpolation according to the extreme shape of the PC axes.

Then, to assess comparisons between groups, Canonical Variate Analyses (CVA) have been performed using the 'CVA' function of the 'Morpho' package' [51]. Eleven datasets were created for mandibular shape comparisons within the total group of patients and controls, between patients and controls for each syndrome independently, as well as between each groups of patients.

Multiple ANalysis Of VAriance (MANOVAs) were performed considering 'type of syndrome' and 'age at CT-scan' as classifiers, considering 90 % of total shape variability (corresponding to ten axes of the PCA).

Statistical analysis

Quantitative data were expressed as mean ± Standard Derivation or median ± Interquartile range and were compared using the Kruskal-Wallis test. $p < 0.05$ was considered as significant.

Results

1. Patients

Forty patients were included into our study: 12 patients with Crouzon syndrome, 12 with Apert syndrome, 12 with Muenke syndrome and 4 with Crouzon syndrome with *acanthosis nigricans*, and 40 age and sex-matched controls. Male/female ratio was 16/24 and mean age at inclusion (date of CT-scan) was 13.7 months ± 11.9, without statistical difference between the four groups (p=0.15). Patients characteristics, types of mutations and of craniosynostosis, and age at CT-scan for each group were summarized in Table 1. Seventeen patients (6/12 in Crouzon, 4/12 in Apert, 4/12 in Muenke, and 3/4 in Crouzon with *acanthosis nigricans* group) had benefited from posterior skull vault expansion prior to the date of CT-scan, at post-operative days 1 or 2. Three patients had severe ventilation disorders requiring temporary tracheostomy (two with Crouzon with *acanthosis nigricans* and one with Crouzon syndrome).

2. Comparative geometric morphometric analysis of mandibular shape

GPA and PCA analyses were performed on the total group of patients and controls. PCA of the mandible shapes showed a clear shape separation of patients and controls along PC2 while PC1 comprised age related shape changes, as confirmed by linear regression tests (r^2=0.42; $p<10^{-4}$). The plots of PC scores and 3D shape changes associated with PC1 and PC2 by morphing the mean mandibular surface model are shown in Figure 2. Mean 3D mandibular shape differed significantly between patients and controls ($p<10^{-3}$). 3D mandibular shape differences obtained after CVA are shown in Figure 3.

2.1. In *FGFR2*-related craniosynostoses

The plots of PC scores and wire frames of the first two PCs and 3D shape changes associated to PC2 for patients and control groups are shown in Figure 4. ANOVA analyses showed significant statistical shape differences along PC2 between patients and controls in Crouzon and Apert groups ($p<10^{-2}$).

Mandibular shape in Crouzon patients was characterized by (1) open gonial angle, (2) short ramus height, (3) narrow inter-gonial and inter-condylar distances and (4) slightly high and prominent symphysis at the level of alveolar bone.

Mandibular shape in Apert patients was characterized by (1) open gonial angle, (2) short ramus height and (3) slightly high and prominent symphysis at both basilar and alveolar levels.

2.2. In *FGFR3*-related craniosynostoses

The plots of PC scores and wire frames of the first two PCs and 3D shape changes associated to PC2 for patients and controls group are shown in Figure 5. ANOVA analyses showed significant statistical shape differences along PC2 between patients and controls in Muenke group ($p<10^{-3}$). The low number of patients in Crouzonodermoskeletal subgroup did not allow ANOVA analysis.

Mandibular shape in Muenke patients was characterized by (1) slightly high and prominent symphysis at the level of basilar border only and (2) open sigmoid notch with anteriorly placed coronoid process and (3) narrow inter-gonial distance.

Mandibular shape in Crouzonodermoskeletal patients was characterized by (1) prominent symphysis at both alveolar and basilar levels and (2) narrow inter-condylar and inter-gonial distance.

2.3. Comparison of mandibular shape between the groups of *FGFR2* and *FGFR3*-craniosynostoses

To analyse shape differences between each patient group , a MANOVA test was performed and showed statistically significant differences between Crouzon and Apert ($p=0.04$), Crouzon and Muenke ($p<10^{-3}$) and Apert and Muenke patients ($p<10^{-3}$). 3D mandibular shape differences between patient groups obtained after CVA are shown in Figure 6.

Short ramus height appeared more pronounced in Apert than in Crouzon syndrome and did not obviously affect patients with *FGFR3*-syndromes. In Crouzon syndrome, condylar processes appeared narrower when compared to Apert and Muenke syndromes. The angular processes were also narrower in Crouzon and Muenke syndromes, when compared with Apert syndrome. Coronoid processes were anteriorly displaced in Muenke syndrome when compared with the other groups. The position of the symphysis did not differ obviously among groups. No statistically significant shape separation was observed between Crouzonodermoskeletal patients (n=4) and the other groups (data not shown).

Discussion

Mandibular shape results from genetic and epigenetic factors, thus explaining the high phenotypic heterogeneity among individuals [52]. Mandibular shape is also constantly modified along life, related to numerous anatomical and functional factors such as dental eruption, tooth loss, mastication, and lingual function [41,42,53]. Determining intrinsic mandibular anomalies in craniosynostosis syndromes is thus a technical challenge, where mandibular shape is also affected by skull base changes.

High genetic variability characterizes Crouzon syndrome, with at least 47 distinct mutations described to date [54], while Apert syndrome is characterized by a very small set of mutations (*FGFR2*^{S252W}, *FGFR2*^{P253R}, and *FGFR2*^{S252F} in a lesser extent) [55,56] and Muenke and Crouzonodermoskeletal syndromes are caused by a unique mutation (*FGFR3*^{P250R} and *FGFR3*^{A391E}, respectively) [10,11]. Although based on a relatively small sample of genotyped patients, our cohort was representative of the main mutations usually reported in these syndromic craniosynostoses. Only four patients diagnosed with the extremely rare Crouzonodermoskeletal syndrome with confirmed A391E mutation could be included in this study.

Our results showed significant distinct mandibular shapes at early ages in Crouzon, Apert, Muenke and Crouzonodermoskeletal syndromes when compared with age and sex-matched controls and highlight genotype-phenotype correspondence in *FGFR2*- and *FGFR3*-related syndromic craniosynostoses. Although Crouzon and Apert patients displayed comparable

315 mandibular shapes (open gonial angle, short ramus height, slightly high and prominent
316 symphysis), anatomical variations were stronger in the Apert than in the Crouzon subgroup,
317 which is consistent with previous findings for the upper third of the face, the midface
318 [3,21,57,58] and the mandible [59,60].
319 Significant differences in mandibular shapes were observed in Muenke and
320 Crouzonodermoskeletal subgroups relative to controls. However, changes did not obviously
321 affect ramus height and gonial angulation, unlike *FGFR2*-craniosynostoses. These
322 morphological differences between *FGFR2*- and *FGFR3*-craniosynostoses reinforce the
323 hypothesis that activating mutations in *FGFR2* and *FGFR3* genes may affect membranous
324 and endochondral ossification processes within different manners, and hence generate
325 variable craniofacial and mandibular phenotypes. Concerning mandibular formation, *FGFR2*
326 and *FGFR3*-activating mutations may have differential intrinsic effects on the primary
327 (Meckel cartilage) and secondary condylar and symphyseal cartilages, then affecting
328 mandibular development and morphology. In addition, it has been shown that patients
329 affected by achondroplasia (linked to activating mutations in *FGFR3* gene), presented
330 defective size and orientation of the ramus [28]. Overall, this underlines the different effects
331 of the distinct mutations in *FGFR3* gene – responsible for craniosynostosis and
332 chondrodysplasia – on mandibular formation and morphology.
333 Of note, we observed anteriorly displaced coronoid processes in Muenke subgroup relative to
334 controls and other patient groups. This morphological feature may be induced by the cranial
335 shape modifications, particularly affecting the temporal region, then influencing temporal
336 muscles dynamics at both temporal and coronoid insertions levels.
337 In all subgroups, tendency for prominent and high symphysis was observed. Symphysis shape
338 is determined by the combined effects of dental eruption and occlusion, and the position of
339 the mandible relative to the maxilla, as well as tongue function and suprahyoid muscles

insertion sites [41, 61]. We could not control all potential influencing factors of mandibular shape in this retrospective study. In addition, we could not confirm that prominent symphysis reflected true prognathism, as all patients had moderate to extreme midfacial retrusion. The severity of midfacial retrusion varies among individuals with reported genotype-phenotype correlations [3]. In fact, midfacial retrusion appeared more pronounced in Apert than in Crouzon syndrome, more obvious in Apert cases carrying *FGFR2*^{S252W} mutation relative to those carrying *FGFR2*^{P253R} mutation, the latter leading to more severe midfacial retrusion than does *FGFR3*^{P250R}, responsible for Muenke syndrome [3,62].

Crouzon syndrome is characterized by its wide spectrum of craniofacial features, from normal phenotype to severe cloverleaf skull malformations. In our series, we also observed high variability of craniosynostosis, from no synostosis at the time of the study (in one patient) to severe cloverleaf skull shape, and moderate to severe fronto-maxillary retrusion. Noticeably, phenotypic features may be absent at birth and evolve gradually during the first years of life [63-65]. However, we observed homogeneous mandibular shapes in the group of Crouzon patients even though six distinct mutations were observed in this group.

Several authors have reported various and sometimes divergent mandibular phenotypic features in *FGFR2*-related syndromic craniosynostoses, in terms of proportions and shapes [23-27,60]. First, these divergent results may be explained by the heterogenous ages at inclusion in the different series. Secondly, mandibular morphology was analysed by various methods, often after craniofacial surgery procedures, thus challenging the comparisons between the studies. Of note, the mandibular shape and particularly intercondylar width, depend on the distance between the condylar fossa on the skull base, as shown in Crouzon and Apert syndromes [27]. Similar results have been found in artificially deformed skulls, where external mechanical constraints had been intentionally exerted on the skull vault with different deforming devices as observed worldwide [66-69]: secondary skull base

365 modifications induced a shift in the position of the glenoid fossa, thus influencing mandibular
366 shape [67,69]. In syndromic craniosynostoses, intrinsic skull base deformations could thus act
367 as potential secondary influencing factors on mandibular shape. We showed a slight
368 narrowing of the condylar processes in Crouzon and Crouzonodermoskeletal syndromes when
369 compared with controls, which was consistent with previous findings [23,27]. This finding
370 thus most probably resulted from the combined effects of (1) repercussions of the vault
371 deformation on the skull base, (2) intrinsic skull base deformations and (3) intrinsic
372 mandibular shape characteristics.
373 Of note, all included CT-scans were performed at early ages before fronto-facial and fronto-
374 orbital surgery, thus ruling out potential effects of surgery on mandibular shape. In fact,
375 fronto-facial surgery involved maxillary advancement [22,70,71] and could thus influence
376 mandibular morphology.
377 Concerning mean age at selected CT-scan, no significant differences were observed between
378 groups. We confirmed by metric measurements, wider angles in Crouzon and Apert patient
379 group when compared with controls ($p=0.03$ and $p=0.003$, respectively). Although mean ages
380 were not statistically different between groups, quantifying mandibular size differences with
381 metric values based on linear measurements would require a different study design, with
382 strictly the same ages in each group, which was not fully the case in our population of
383 growing children. We aimed to detect shape differences among groups, independently of
384 mandibular size, which varies among individuals, particularly with age. We thus performed a
385 General Procrustes Analysis, as it allows valid shape comparisons for objects of different
386 sizes and detection of proportional changes of one anatomical region relatively to another.
387 Concerning results of PCA, while PC1 comprised age-related changes, PC2 clearly separated
388 patients from controls, thus excluding the sole effect of age on mandibular morphological
389 variations. Finally, comparisons between each patients group showed statistically significant

morphological differences between Crouzon and Apert, Crouzon and Muenke, and Apert and Muenke patients. Overall, our results strengthen the hypothesis that mandibular shape in *FGFR*-related syndromic craniosynostoses results from the *FGFR* activating mutation disturbing ossification processes and reinforce the hypothesis of genotype-phenotype correspondence. No statistical difference was found for morphological comparisons between Crouzonodermoskeletal patients and the other groups, most probably due to the small sample of this extremely rare syndromic craniosynostosis.

Early tracheostomy was required for two patients with Crouzonodermoskeletal syndrome and one patient with Crouzon syndrome. These patients presented severe midfacial retrusion, and the mandible appeared as 'prognathic' relative to the maxilla. Although this small sample size did not allow statistical comparisons, linear measurements of the mandibles could not reveal significant differences between patients with or without tracheostomy.

FGFR-related syndromic craniosynostoses are due to gain-of-function activating mutations of *FGFR* genes. The impact of a constitutive activation in *FGFR2* and *FGFR3* on endochondral ossification has been first shown for long bones (*FGFR3*) and skull base synchondrosis (*FGFR2* and *FGFR3*) with altered chondrocyte proliferation and differentiation [72-80]. The impact of activating mutations in *FGFR2* and *FGFR3* on mandibular formation has been more recently studied [28,82-84]. Mandibular bone is formed by intramembranous ossification induced before birth at the site of Meckel cartilage, and by endochondral ossification at the site of condylar, angular and symphyseal cartilages, serving as growth centres after birth [38,81]. Mandibular shape differences have been observed in mouse models for Apert ($Fgfr2^{+/S252W}$, and $Fgfr2^{+/P253R}$) and Crouzon syndromes ($Fgfr2c^{C342Y/+}$), with affected ramus morphology in all models. The greatest magnitude of morphological changes was for $Fgfr2^{+/S252W}$ mice, while the Crouzon model showed the most limited changes; interestingly, anterior body shape changes were only seen in this Crouzon model [82]. This study also

demonstrated increased Meckel cartilage volume and increased proliferation of osteoblasts and chondrocytes forming this cartilage in *Fgfr2*$^{+/S252W}$ mice [82]. Concerning *FGFR3* activating mutations, a mouse model for Muenke syndrome, *Fgfr3*^{P244R}, disturbed temporomandibular joint developmental processes [83,84]. A mouse model for achondroplasia, *Fgfr3*$^{G380R/G380R}$, presented structural anomalies of primary (Meckel) and secondary cartilages of the condylar region, demonstrating the implication of *FGFR3* in both membranous and endochondral ossification [28].

FGFR2 and *FGFR3* code for a tyrosine kinase receptor. FGF receptors have an extracellular ligand-binding portion composed of immunoglobulin-like domains (IgI, IgII, and IgIII), a transmembrane region, and intracellular tyrosine kinase domains (TK1 and TK2) [8,12]. The FGF family, composed of at least 22 known FGF ligands, binds an FGFR, resulting in receptor monomer dimerization, activation of kinase domains and phosphorylation of the receptor [8]. The impact of the mutations within the FGF receptor extracellular ligand binding domain may also be an explanation for the variability of the mandibular phenotype: while mutations within the IgII-IgIII linker region result in altered ligand-binding specificity and/or affinity as in Apert and Muenke syndrome [85-89], mutations within the IgIII linker region result in aberrant intermolecular disulfide bonds between unpaired cysteine residues leading to the constitutive activation of the receptor, as in Crouzon syndrome [89-91]. Crouzonodermoskeletal syndrome is due to a single point mutation (pAla391Glu) localized in transmembrane domain of FGFR3 resulting in an increase of the phosphorylation level of FGFR3 independently of the presence of ligand [11,92]. Further molecular and biological studies are required to better clarify the affected signalling pathways downstream FGF receptors involved in the craniofacial phenotype of *FGFR*-related craniosynostoses.

Mandibular development is affected in various malformation syndromes without craniosynostosis such as in Robin sequence, Treacher Collins or Nager syndromes, due to

mutations in distinct genes, in which mandibular hypoplasia and retrognathia are observed within various degrees of severity [93,94]. Comparing mandibular shapes between craniosynostosis and non-craniosynostosis craniofacial syndromes may help in the understanding of the intrinsic effects of the different mutations on mandibular development and morphology. In our series, we aimed to analyse mandibular shapes at early ages to avoid potential confounding factors related to the effects of surgery on mandibular shape. As mandibular shape varies all along growth, especially the condylar region which is a major center of post-natal growth, analysing mandibular shape at the end of the growth when the condyle achieved a complete ossification, would be required to confirm changes in mandibular vertical height, as we observed in *FGFR2*-craniosynostosis. In fact, mandibular vertical height may be underestimated in the youngest patients, before complete ossification of the secondary condylar cartilages occurs [95].

To conclude, our results demonstrated distinct mandibular shapes at early ages in different subtypes of *FGFR2*- (Crouzon and Apert syndromes) and *FGFR3*-related syndromic craniosynostoses (Muenke and Crouzonodermoskeletal syndromes) and reinforce the hypothesis of genotype-phenotype correspondence concerning mandibular morphology. Studies on larger cohorts and integration of skull base and midface morphological data in the analysis of mandibular shape are required to determine whether the mandible is less subjected to interindividual variations than other craniofacial features. Mandibular shape would therefore be a valid clinical parameter in the characterization of *FGFR*-related craniosynostoses.

Table I. Patient's characteristics: number per group, sex ratio, type of mutation and of craniosynostosis, and age at CT-scan

Patient group	Patient's number Sex ratio (F/M)	Mutations	Types of craniosynostosis (n)	Median age (IQR) at CT-scan (months)
Crouzon *FGFR2*	12 (7/5)	Cys342Tyr (n=4) Tyr105Cys (n=2) Cys278Phe (n=2) Gly338Glu (n=2) Ser267Pro (n=1) Arg347Cys (n=1)	BCS + MS + SS + BLS (2), BCS + MS + SS (1), BCS + SS + BLS (1), BCS + SS (1), BCS (1), UCS (1), UCS + partial BLS (1), UCS + MCS (1), SS (1), BLS (1), None (1)	11 (16.9)
Apert *FGFR2*	12 (6/6)	Ser252Trp (n=11) Pro253Arg (n=1)	BCS (9), BCS + SS (1), UCS (1), MS + SS (1)	8.9 (9.2)
Muenke *FGFR3*	12 (9/3)	Pro250Arg (n=12)	BCS (10), UCS (2)	6.8 (4.8)
CAN *FGFR3*	4 (3/1)	Ala391Glu (n=4)	BCS (2), BCS + SS (1), UCS + BLS (1)	22.7 (12.6)

CAN: Crouzon with acanthosis nigricans; IQR: Inter Quartile Range

BCS: bilateral coronal synostosis, UCS: unilateral coronal synostosis, SS: sagittal synostosis, MS: metopic synostosis; BLS: bilateral lambdoid synostosis.

* Frontofacial or frontoorbital advancement (performed after the studied CT-scan for all patients).

Figure 1. Landmarks on the buccal and lingual sides digitized on hemi mandibles surface three-dimensional models: a: anatomical landmarks (31); b: curves (11) (based on previous studies [41,42]).

A. Anatomical landmarks (n=31)

AntGo	Antegonial
CoAnt	Anterior border of the articular surface of the condyle
CoExt	External border of the articular surface of the condyle
CoInt	Medial border of the articular surface of the condyle
CoPost	Posterior border of the articular surface of the condyle
Cor	Coronoid process (highest point)
Col	Condylar neck (highest concavity)
Gn	Gnathion
Go	Gonion
InfDe	Infradentale (most superior point of the alveolar bone at the inter incisive midline)
Me	Mental point
MeSp	Mental spine
Pog	Pogonion

RetroMolExt	Retromolar external
RetroMolInt	Retromolar internal
Sig	Sigmoid notch (highest concavity)
Spix	Spix spine

All the landmarks were positioned bilaterally except midline landmarks (InfDe, Pog, MeSp).

B. Curves (n=11)

Curve	Course	Number of sliding semi-landmarks per curve
Anterior Ramus curve	from 'Cor' to the most inferior point of the anterior edge of the ramus	7
Basilar Border curve	from 'CoPost', all along the posterior border of the neck, ramus, corpus, to the most inferior point of the symphysis	20
Coronoid curve	from 'CoAnt' to 'Cor'	10
Inner Alveolar curve	from the most posterior point of the alveolar bone, running along the lingual side of the alveolar curve, to the inter incisive point	15
Outer Alveolar curve	from the most posterior point of the alveolar bone, running along the vestibular side of the alveolar curve, to the point 'InfDe'	15
Symphysis	from 'InfDe', surrounds the basilar border, and ends at the inter incisive point at lingual side	20

All curves were positioned bilaterally except Symphysis curve (midline)

Figure 2. Plots of Principal Components (PC) scores for PC1 and PC2 with corresponding variances (in %) (A), and (B) 3D shape changes associated with PC1 and PC2 by morphing the extreme mandibular surface model (blue: negative values; red: positive values). A: patients (square box); controls (round box): AP: Apert Patients ; AC: Controls for Apert Patients; CP: Crouzon Patients; CC: Controls for Crouzon Patients; CANP: CAN (Crouzonodermoskeletal) patients; CANC: Controls for CAN Patients; MP: Muenke Patients; MC: Controls for Muenke Patients.

Figure 3. Plots of Canonical Variate (CV) scores (A) and 3D mandibular shape associated to CV1 and CV2 (B) (n=40 patients: 12 with Crouzon syndrome, 12 with Apert syndrome, 12 with Muenke syndrome, 4 with Crouzonodermoskeletal syndrome and n=40 age and sex-matched controls).

A: patients (square box); controls (round box): AP: Apert Patients ; AC: Controls for Apert Patients; CP: Crouzon Patients; CC: Controls for Crouzon Patients; CANP: CAN (Crouzonodermoskeletal) patients; CANC: Controls for CAN Patients; MP: Muenke Patients; MC: Controls for Muenke Patients.

B: The dots represent the extreme values (green: negative values; red: positive values) of each anatomical landmark and sliding curve semi-landmark.

Figure 4. Comparison of mandibular shape between patients with *FGFR2*-craniosynostoses and controls: plots of Principal Components (PC) scores for PC1 and PC2 with corresponding variances (in %) (patients (magenta), controls (black)), and 3D shape changes associated with PC2 by morphing the extreme mandibular surface model (blue: negative values; red: positive values) for A: Crouzon group (n=12 patients; n=12 controls); B: Apert group (n=12 patients; n=12 controls).

Figure 5. Comparison of mandibular shape between patients with *FGFR3*-craniosynostoses and controls: plots of Principal Components (PC) scores for PC1 and PC2 with corresponding variances (in %) (patients (magenta), controls (black)), and 3D shape changes associated with PC2 by morphing the extreme mandibular surface model (blue: negative values; red: positive values) for A: Muenke group (n=12 patients; n=12 controls); B: CAN (Crouzonodermoskeletal) group (n=4 patients; n=4 controls).

Figure 6. 3D representations showing mandibular shape variations between patient groups using Canonical Variate Analysis, for A: Crouzon vs Apert group; B: Crouzon vs Muenke group; C: Apert vs Muenke group. The dots represent the extreme values (green: negative values; red: positive values) of each anatomical landmark and sliding curve semi-landmark (n=12 patients; n=12 controls for each group).
All comparisons were statistically significant ($p<0.05$).

Acknowledgements

We thank Drs PA Diner, C Tomat, S James and Pr M Zerah for their contribution to the management of the patients.

References

[1] Johnson D, Wilkie AO. Craniosynostosis. Eur J Hum Genet. 2011 Apr;19(4):369-76. doi: 10.1038/ejhg.2010.235. Epub 2011 Jan 19.

[2] Heuzé Y, Holmes G, Peter I, Richtsmeier JT, Jabs EW. Closing the Gap: Genetic and Genomic Continuum from Syndromic to Nonsyndromic Craniosynostoses. Curr Genet Med Rep. 2014 Sep 1;2(3):135-145.

[3] Heuze, Y., Martinez-Abadias, N., Stella, J. M., Arnaud, E., Collet, C., Garcia, Fructuoso, G., Alamar, M., Lo, L. J., Boyadjiev, S. A., Di Rocco, F., *et al*. Quantification of facial skeletal shape variation in fibroblast growth factor receptor-related craniosynostosis syndromes. Birth Defects Res. A Clin. Mol. Teratol. 2014 100, 250-259.

[4] Flaherty K, Singh N, Richtsmeier JT. Understanding craniosynostosis as a growth disorder. Wiley Interdiscip Rev Dev Biol. 2016 Jul;5(4):429-59. doi: 10.1002/wdev.227.

[5] Armand T, Schaefer E, Di Rocco F, Edery P, Collet C, Rossi M. Genetic bases of craniosynostoses: An update. Neurochirurgie. 2019 Nov;65(5):196-201. doi: 10.1016/j.neuchi.2019.10.003. Epub 2019 Oct 9.

570 [6] Lattanzi W, Barba M, Di Pietro L, Boyadjiev SA. Genetic advances in craniosynostosis.
571 Am J Med Genet A. 2017;173(5):1406- 29.
572 [7] Wilkie AO, Slaney SF, Oldridge M, Poole MD, Ashworth GJ, Hockley AD, Hayward RD,
573 David DJ, Pulleyn LJ, Rutland P, *et al*. Apert syndrome results from localized mutations of
574 FGFR2 and is allelic with Crouzon syndrome. Nat Genet. 1995 Feb;9(2):165-72.
575 [8] Azoury SC, Reddy S, Shukla V, Deng CX. Fibroblast Growth Factor Receptor 2 (FGFR2)
576 Mutation Related Syndromic Craniosynostosis. Int J Biol Sci. 2017 Nov 2;13(12):1479-1488.
577 doi: 10.7150/ijbs.22373.
578 [9] Rutland P, Pulleyn LJ, Reardon W, Baraitser M, Hayward R, Jones B, Malcolm S, Winter
579 RM, Oldridge M, Slaney SF, *et al*. Identical mutations in the FGFR2 gene cause both Pfeiffer
580 and Crouzon syndrome phenotypes. Nat Genet. 1995 Feb;9(2):173-6.
581 [10] Muenke M, Gripp KW, McDonald-McGinn DM, Gaudenz K, Whitaker LA, Bartlett SP,
582 *et al*. A unique point mutation in the fibroblast growth factor receptor 3 gene (FGFR3) defines
583 a new craniosynostosis syndrome. Am J Hum Genet. 1997 Mar;60(3):555-64.
584 [11] Meyers GA, Orlow SJ, Munro IR, Przylepa KA, Jabs EW. Fibroblast growth factor
585 receptor 3 (FGFR3) transmembrane mutation in Crouzon syndrome with acanthosis nigricans.
586 Nat Genet. 1995 Dec;11(4):462-4.
587 [12] Robin NH, Falk MJ, Haldeman-Englert CR. FGFR-Related Craniosynostosis
588 Syndromes. In: Adam MP, Ardinger HH, Pagon RA, Wallace SE, Bean LJH, Stephens K,
589 Amemiya A, editors. GeneReviews® [Internet]. Seattle (WA): University of Washington,
590 Seattle; 1993-2020.
591 [13] Schweitzer, DN, Graham, JM, Lachman, RS, Jabs, EW, Okajima, K, Przylepa, KA,
592 Wilcox WR. Subtle radiographic findings of achondroplasia in patients with Crouzon
593 syndrome with acanthosis nigricans due to an Ala391Glu substitution in FGFR3. American
594 Journal of Medical Genetics. 2001 98(1), 75–91.

595 [14] Arnaud-López, L, Fragoso, R., Mantilla-Capacho, J, Barros-Núñez, P. Crouzon with
596 acanthosis nigricans: Further delineation of the syndrome. Clinical Genetics, 2007 72(5),
597 405–410.
598 [15] Montero A, Okada Y, Tomita M, Ito M, Tsurukami H, Nakamura T, Doetschman T,
599 Coffin JD, Hurley MM. Disruption of the fibroblast growth factor-2 gene results in decreased
600 bone mass and bone formation. J Clin Invest. 2000 Apr;105(8):1085-93.
601 [16] Ornitz DM. FGF signaling in the developing endochondral skeleton. Cytokine Growth
602 Factor Rev. 2005 Apr;16(2):205-13.
603 [17] David M. Ornitz and Pierre J. Marie. Fibroblast growth factor signaling in skeletal
604 development and disease. Genes Dev. 2015 29: 1463-1486; doi:10.1101/gad.266551.115.
605 [18] Ornitz DM, Marie PJ. Fibroblast growth factors in skeletal development. Curr Top Dev
606 Biol. 2019;133:195-234. doi: 10.1016/bs.ctdb.2018.11.020.
607 [19] Cunningham ML, Seto, ML, Ratisoontorn, C, Heike CL & Hing, AV. Syndromic
608 craniosynostosis: from history to hydrogen bonds. Orthod. Craniofac. AtRes. 2007 10, 67-81.
609 [20] Holmes G, O'Rourke C, Motch Perrine SM, Lu N, van Bakel H, Richtsmeier JT, Jabs
610 EW. Midface and upper airway dysgenesis in FGFR2-related craniosynostosis involves
611 multiple tissue-specific and cell cycle effects. Development. 2018 Oct 5;145(19). pii:
612 dev166488. doi: 10.1242/dev.166488.
613 [21] Way BLM, Khonsari RH, Karunakaran T, Nysjö J, Nyström I, Dunaway DJ, Evans RD,
614 Hayward RD, Britto JA. Correcting Exorbitism by Monobloc Frontofacial Advancement in
615 Crouzon-Pfeiffer Syndrome: An Age-Specific, Time-Related, Controlled Study. Plast
616 Reconstr Surg. 2019 Jan;143(1):121e-132e. doi: 10.1097/PRS.0000000000005105.
617 [22] Bouaoud J, Hennocq Q, Paternoster G, James S, Arnaud E, Khonsari RH. Excessive
618 ossification of the bandeau in Crouzon and Apert syndromes. J Craniomaxillofac Surg. 2020
619 Apr;48(4):376-382

620 [23] Boutros S, Shetye PR, Ghali S, Carter CR, McCarthy JG, Grayson BH. Morphology and
621 growth of the mandible in Crouzon, Apert, and Pfeiffer syndromes. J Craniofac Surg. 2007
622 Jan;18(1):146-50.
623 [24] Wink JD, Bastidas N, Bartlett SP. Analysis of the long-term growth of the mandible in
624 Apert syndrome. J Craniofac Surg. 2013 Jul;24(4):1408-10. doi:
625 10.1097/SCS.0b013e31828dcf09.
626 [25] Kolar JC, Ditthakasem K, Fearon JA. Long-Term Evaluation of Mandibular Growth in
627 Children With FGFR2 Mutations. J Craniofac Surg. 2017 May;28(3):709-712. doi:
628 10.1097/SCS.0000000000003494.
629 [26] Khominsky A, Yong R, Ranjitkar S, Townsend G, Anderson PJ. Extensive phenotyping
630 of the orofacial and dental complex in Crouzon syndrome. Arch Oral Biol. 2018 Feb;86:123-
631 130. doi: 10.1016/j.archoralbio.2017.10.022.
632 [27] Lu X, Sawh-Martinez R, Forte AJ, Wu R, Cabrejo R, Wilson A, Steinbacher DM,
633 Alperovich M, Alonso N, Persing JA. Mandibular Spatial Reorientation and Morphological
634 Alteration of Crouzon and Apert Syndrome. Ann Plast Surg. 2019 Nov;83(5):568-582. doi:
635 10.1097/SAP.0000000000001811.
636 [28] Biosse Duplan M, Komla-Ebri D, Heuzé Y, Estibals V, Gaudas E, Kaci N, Benoist-
637 Lasselin C, Zerah M, Kramer I, Kneissel M, Porta DG, Di Rocco F, Legeai-Mallet L.
638 Meckel's and condylar cartilages anomalies in achondroplasia result in defective development
639 and growth of the mandible. Hum Mol Genet. 2016 Jul 15;25(14):2997-3010.
640 [29] Noden, DM. The role of the neural crest in patterning of avian cranial
641 skeletal, connective, and muscle tissues. Dev. Biol. 1983 96, 144-165. doi:10.1016/
642 0012-1606(83)90318-4.
643 [30] Couly, G, Grapin-Botton, A, Coltey, P and Le Douarin, NM. The regeneration of the
644 cephalic neural crest, a problem revisited: the regenerating cells originate from the

645 contralateral or from the anterior and posterior neural fold. Development. 1996 122, 3393-
646 1407.
647 [31] Chai Y, Jiang X, Ito Y, Bringas P Jr, Han J, Rowitch DH, Soriano P, McMahon AP,
648 Sucov HM. Fate of the mammalian cranial neural crest during tooth and mandibular
649 morphogenesis.
650 Development. 2000 Apr;127(8):1671-9.
651 [32] Depew MJ, Lufkin T and Rubenstein, J.LR. Specification of jaw subdivisions by Dlx
652 genes. Science. 2002 298, 381-385. doi:10.1126/science.1075703
653 [33] Frisdal, A and Trainor PA. Development and evolution of the pharyngeal
654 apparatus. Wiley Interdiscip. Rev. Dev. Biol. 2014 3, 403-418. doi:10.1002/wdev.147.
655 [34] Lipski M, Tomaszewska IM, Lipska W, Lis GJ, Tomaszewski KA. The mandible and its
656 foramen: anatomy, anthropology, embryology and resulting clinical implications. Folia
657 Morphol. (Warsz). 2013 Nov;72(4):285-92
658 [35] Rice DP, Rice R, Thesleff I. Fgfr mRNA isoforms in craniofacial bone development.
659 Bone. 2003 Jul;33(1):14-27.
660 [36] Havens BA, Rodgers B, Mina M. Tissue-specific expression of Fgfr2b and Fgfr2c
661 isoforms, Fgf10 and Fgf9 in the developing chick mandible. Arch Oral Biol. 2006
662 Feb;51(2):134-45. Epub 2005 Aug 18.
663 [37] Havens BA, Velonis D, Kronenberg MS, Lichtler AC, Oliver B, Mina M. Roles of
664 FGFR3 during morphogenesis of Meckel's cartilage and mandibular bones. Dev Biol. 2008
665 Apr 15;316(2):336-49. doi: 10.1016/j.ydbio.2008.01.035.
666 [38] Parada C, Chai Y. Mandible and Tongue Development. Curr Top Dev Biol.
667 2015;115:31-58. doi: 10.1016/bs.ctdb.2015.07.023.

[39] Yu K, Karuppaiah K, Ornitz DM. Mesenchymal fibroblast growth factor receptor signaling regulates palatal shelf elevation during secondary palate formation. Dev Dyn. 2015 Nov;244(11):1427-38. doi: 10.1002/dvdy.24319.

[40] Fedorov A., Beichel R., Kalpathy-Cramer J., Finet J., Fillion-Robin J-C., Pujol S., Bauer C., Jennings D., Fennessy F.M., Sonka M., Buatti J., Aylward S.R., Miller J.V., Pieper S., Kikinis R. 3D Slicer as an Image Computing Platform for the Quantitative Imaging Network. Magn Reson Imaging. 2012 Nov;30(9):1323-41. PMID: 22770690. PMCID: PMC3466397.

[41] Coquerelle M, Prados-Frutos JC, Benazzi S, Bookstein FL, Senck S, Mitteroecker P, Weber GW. Infant growth patterns of the mandible in modern humans: a closer exploration of the developmental interactions between the symphyseal bone, the teeth, and the suprahyoid and tongue muscle insertion sites. J Anat. 2013 Feb;222(2):178-92. doi: 10.1111/joa.12008.

[42] Guevara Perez SV, de la Rosa Castolo G, Thollon L, Behr M. A 3D characterization method of geometric variation in edentulous mandibles. Morphologie. 2018 Dec;102(339):255-262. doi: 10.1016/j.morpho.2018.08.001.

[43] Gunz P, Mitteroecker P. Semilandmarks: a method for quantifying curves and surfaces. Hystrix, the Italian Journal of Mammalogy. 2013;24(1):103-109. doi:10.4404/hystrix-24.1-6292.

[44] Klingenberg CP. MorphoJ: an integrated software package for geometric morphometrics. Mol Ecol Resour. 2011 Mar;11(2):353-7. doi: 10.1111/j.1755-0998.2010.02924.x. Epub 2010 Oct 5. PMID: 21429143.

[45] Zelditch ML, Swiderski DL, Sheets HD. Geometric Morphometrics for Biologists: A Primer. Academic Press, Cambridge (2012).

[46] R Core Team (2019). R: A language and environment for statistical computing. R Foundation for Statistical Computing, Vienna, Austria. URL https://www.R-project.org/

692 [47] Rohlf FJ, Slice D. Extensions of the Procrustes method for the optimal superimposition
693 of landmarks. Syst. Zool., 1990;39(1):40-59.
694 [48] Adams DC, Collyer ML, and Kaliontzopoulou A. 2018. Geomorph: Software for
695 geometric morphometric analyses. R package version 3.0.6. https://cran.r
696 project.org/package=geomorph.
697 [49] Baylac, M., & Frieß, M. (2005). Fourier descriptors, Procrustes superimposition, and
698 data dimensionality: an example of cranial shape analysis in modern human populations. In
699 Modern morphometrics in physical anthropology (pp. 145-165). Springer, Boston, MA.
700 [50] Bookstein FL. Principal warps: Thin-plate splines and the decomposition of
701 deformations. IEEE Transactions on pattern analysis and machine intelligence. 1989;11(6),
702 567-585.
703 [51] Schlager S. “Morpho and Rvcg - Shape Analysis in R.” In Zheng G, Li S, Szekely G
704 (eds.). Statistical Shape and Deformation Analysis, 217-256. Academic Press. 2017. ISBN
705 9780128104934.
706 [52] Atchley WR and Hall BK. A model for development and evolution of complex
707 morphological structures. Biol. Rev. Camb. Philos. Soc. 1991 ;66, 101-157.
708 doi:10.1111/j.1469-185X.1991.tb01138.x.
709 [53] Bastir M, O’Higgins P, Rosas A. Facial ontogeny in Neanderthals and modern humans.
710 Proceedings of the Royal Society. Biol Sci 2007;274:1125—32.
711 [54] Passos-Bueno MR, Sertié AL, Jehee FS, Fanganiello R, Yeh E. Genetics of
712 craniosynostosis: genes, syndromes, mutations and genotype-phenotype correlations. Front
713 Oral Biol. 2008;12:107-143. doi: 10.1159/000115035.
714 [55] Slaney SF, Oldridge M, Hurst J a, Moriss-Kay GM, Hall CM, Poole MD. *et al*.
715 Differential effects of FGFR2 mutations on syndactyly and cleft palate in Apert syndrome.
716 Am J Hum Genet. 1996;58(5):923–32

[56] Ko JM. Genetic syndromes associated with craniosynostosis. J Korean Neurosurg Soc. 2016;59(3):187–91.

[57] Kreiborg S, Cohen MM Jr. Is craniofacial morphology in Apert and Crouzon syndromes the same? Acta Odontol Scand. 1998;56:339–341.

[58] Levasseur J, Nysjö J, Sandy R, Britto JA, Garcelon N, Haber S, Picard A, Corre P, Odri GA, Khonsari RH. Orbital volume and shape in Treacher Collins syndrome. J Craniomaxillofac Surg. 2018 Feb;46(2):305-311. doi: 10.1016/j.jcms.2017.11.028.

[59] Costaras-Volarich M, Pruzansky S. Is the mandible intrinsically different in Apert and Crouzon syndromes? Am J Orthod.1984;85:475–487.

[60] Elmi P, Reitsma JH, Buschang PH, Wolvius EB, Ongkosuwito EM. Mandibular asymmetry in patients with the Crouzon or Apert syndrome. Cleft Palate Craniofac J. 2015 May;52(3):327-35. doi: 10.1597/13-143.

[61] Ahn MS, Shin SM, Yamaguchi T, et al. Relationship between the maxillofacial skeletal pattern and the morphology of the mandibular symphysis: Structural equation modeling. Korean J Orthod. 2019;49(3):170-180. doi:10.4041/kjod.2019.49.3.170.

[62] Ridgway EB, Wu JK, Sullivan SR, Vasudavan S, Padwa BL, Rogers GF, *et al*. Craniofacial growth in patients with FGFR3Pro250Arg mutation after fronto-orbital advancement in infancy. J Craniofac Surg. 2011 22:455-461.

[63] Lajeunie E, Cameron R, El Ghouzzi V, *et al*. Clinical variability in patients with Apert's syndrome. J Neurosurg. 1999;90:443–447.

[64] Connolly JP, Gruss J, Seto ML, *et al*. Progressive postnatal craniosynostosis and increased intracranial pressure. Plast Reconstr Surg. 2004;113:1313–1323.

[65] Hoefkens MF, Vermeij-Keers C, Vaandrager JM. Crouzon syndrome: phenotypic signs and symptoms of the postnatally expressed subtype. J Craniofac Surg. 2004;15:233–240. discussion 241–242.

[66] Dingwall EJ (1931). Artificial cranial deformation—A contribution to the study of ethnic mutilation. London: John Bale, Sons & Danielsson, Ltd.

[67] Cottin M, Khonsari RH, Friess M. Assessing cranial plasticity in humans: The impact of artificial deformation on masticatory and basicranial structures. Comptes Rendus Palevol Volume 16, Issues 5–6, August–September 2017, Pages 545-556.

[68] Püschel TA, Friess M, Manríquez G. Morphological consequences of artificial cranial deformation: Modularity and integration. PLoS One. 2020 Jan 24;15(1):e0227362. doi: 10.1371/journal.pone.0227362. eCollection 2020.

[69] Ferros I, Mora MJ, Obeso IF, Jimenez P, Martinez-Insua A. Relationship between the cranial base and the mandible in artificially deformed skulls. Orthod Craniofac Res. 2016 Nov;19(4):222-233. doi: 10.1111/ocr.12128. Epub 2016 Aug 10.

[70] Morice A, Paternoster G, Ostertag A, James S, Cohen-Solal M, Khonsari RH, Arnaud E. Anterior Skull Base and Pericranial Flap Ossification after Frontofacial Monobloc Advancement. Plast Reconstr Surg. 2018 Feb;141(2):437-445.

[71] Khonsari RH, Haber S, Paternoster G, Fauroux B, Morisseau-Durand MP, Cormier-Daire V, Legeai-Mallet L, James S, Hennocq Q, Arnaud E. The influence of fronto-facial monobloc advancement on obstructive sleep apnea: An assessment of 109 syndromic craniosynostoses cases. J Craniomaxillofac Surg. 2020 Apr. doi.org/10.1016/j.jcms.2020.04.001.

[72] Segev O, Chumakov I, Nevo Z, Givol D, Madar-Shapiro L, Sheinin Y, Weinreb M, Yayon A. Restrained chondrocyte proliferation and maturation with abnormal growth plate vascularization and ossification in human FGFR-3(G380R) transgenic mice. Hum Mol Genet. 2000 Jan 22;9(2):249-58.

[73] Yu K, Xu J, Liu Z, Sosic D, Shao J, Olson EN, Towler DA, Ornitz DM. Conditional inactivation of FGF receptor 2 reveals an essential role for FGF signaling in the regulation of osteoblast function and bone growth. Development. 2003 Jul;130(13):3063-74.

767 [74] Wang Q, Green RP, Zhao G, Ornitz DM. Differential regulation of endochondral bone
768 growth and joint development by FGFR1 and FGFR3 tyrosine kinase domains.Development.
769 2001 Oct;128(19):3867-76.
770 [75] Legeai-Mallet L, Benoist-Lasselin C, Munnich A, Bonaventure J. Overexpression of
771 FGFR3, Stat1, Stat5 and p21Cip1 correlates with phenotypic severity and defective
772 chondrocyte differentiation in FGFR3-related chondrodysplasias. Bone. 2004 Jan;34(1):26-
773 36.
774 [76] Yin L, Du X, Li C, Xu X, Chen Z, Su N, Zhao L, Qi H, Li F, Xue J, Yang J, Jin M, Deng
775 C, Chen L. A Pro253Arg mutation in fibroblast growth factor receptor 2 (Fgfr2) causes
776 skeleton malformation mimicking human Apert syndrome by affecting both chondrogenesis
777 and osteogenesis. Bone. 2008 Apr;42(4):631-43. doi: 10.1016/j.bone.2007.11.019. Epub 2008
778 Jan 31.
779 [77] Matsushita T, Wilcox WR, Chan YY, Kawanami A, Bükülmez H, Balmes G, Krejci P,
780 Mekikian PB, Otani K, Yamaura I, Warman ML, Givol D, Murakami S. FGFR3 promotes
781 synchondrosis closure and fusion of ossification centers through the MAPK pathway. Hum
782 Mol Genet. 2009 Jan 15;18(2):227-40. doi: 10.1093/hmg/ddn339.
783 [78] Di Rocco F, Biosse Duplan M, Heuzé Y, Kaci N, Komla-Ebri D, Munnich A, Mugniery
784 E, Benoist-Lasselin C, Legeai-Mallet L. FGFR3 mutation causes abnormal membranous
785 ossification in achondroplasia. Hum Mol Genet. 2014 Jun 1;23(11):2914-25. doi:
786 10.1093/hmg/ddu004. Epub 2014 Jan 12.
787 [79] Pannier S, Mugniery E, Jonquoy A, Benoist-Lasselin C, Odent T, Jais JP, Munnich A,
788 Legeai-Mallet L. Delayed bone age due to a dual effect of FGFR3 mutation in
789 Achondroplasia. Bone. 2010 Nov;47(5):905-15. doi: 10.1016/j.bone.2010.07.020. Epub 2010
790 Jul 29.

[80] Mugniery E, Dacquin R, Marty C, Benoist-Lasselin C, de Vernejoul MC, Jurdic P, Munnich A, Geoffroy V, Legeai-Mallet L. An activating Fgfr3 mutation affects trabecular bone formation via a paracrine mechanism during growth. Hum Mol Genet. 2012 Jun 1;21(11):2503-13. doi: 10.1093/hmg/dds065. Epub 2012 Feb 24.

[81] Roberts WE and Hartsfield JK. Bone development and function: genetic and environmental mechanisms. Semin. Orthod, 2004 10, 100–122.

[82] Motch Perrine SM, Wu M, Stephens NB, Kriti D, van Bakel H, Jabs EW, Richtsmeier JT. Mandibular dysmorphology due to abnormal embryonic osteogenesis in FGFR2-related craniosynostosis mice. Dis Model Mech. 2019 May 30;12(5). pii: dmm038513. doi: 10.1242/dmm.038513.

[83] Twigg SR, Healy C, Babbs C, Sharpe JA, Wood WG, Sharpe PT, Morriss-Kay GM, Wilkie AO. Skeletal analysis of the Fgfr3(P244R) mouse, a genetic model for the Muenke craniosynostosis syndrome. Dev Dyn. 2009 Feb;238(2):331-42. doi: 10.1002/dvdy.21790.

[84] Yasuda T, Nah HD, Laurita J, Kinumatsu T, Shibukawa Y, Shibutani T, Minugh-Purvis N, Pacifici M, Koyama E. Muenke syndrome mutation, FgfR3P^{244}R, causes TMJ defects. J Dent Res. 2012 Jul;91(7):683-9. doi: 10.1177/0022034512449170. Epub 2012 May 23.

[85] Anderson J, Burns HD, Enriquez-Harris P, Wilkie AO, Heath JK. Apert syndrome mutations in fibroblast growth factor receptor 2 exhibit increased affinity for FGF ligand. Human molecular genetics. 1998; 7(9), 1475-1483.

[86] Yu K, Herr AB, Waksman G, Ornitz DM. Loss of fibroblast growth factor receptor 2 ligand-binding specificity in Apert syndrome. Proc Natl Acad Sci U S A. 2000; 97:14536–14541.

[87] Ibrahimi OA, Eliseenkova AV, Plotnikov AN, Yu K, Ornitz, DM, Mohammadi M. Structural basis for fibroblast growth factor receptor 2 activation in Apert syndrome. Proc Natl Acad Sci U S A. 2001; 98:7182–7187.

816 [88] Ibrahimi OA, Zhang F, Eliseenkova AV, *et al*. Biochemical analysis of pathogenic
817 ligand-dependent FGFR2 mutations suggests distinct pathophysiological mechanisms for
818 craniofacial and limb abnormalities. Hum Mol Genet. 2004; 13:2313–2324.
819 [89] Neilson KM, Friesel R. Ligand-independent activation of fibroblast growth factor
820 receptors by point mutations in the extracellular, transmembrane, and kinase domains. J Biol
821 Chem. 1996; 271:25049–25057.
822 [90] Mangasarian K, Li Y, Mansukhani A, Basilico C. Mutation associated with Crouzon
823 syndrome causes ligand-independent dimerization and activation of FGF receptor-2. J Cell
824 Physiol. 1997; 172:117–125.
825 [91] Robertson SC, Meyer AN, Hart KC, *et al*. Activating mutations in the extracellular
826 domain of the fibroblast growth factor receptor 2 function by disruption of the disulfide bond
827 in the third immunoglobulin-like domain. Proc Natl Acad Sci U S A. 1998; 95:4567–4572.
828 [92] Chen F, Degnin C, Laederich M, Horton W, Hristova K. The A391E mutation enhances
829 FGFR3 activation in the absence of ligand. Biochim Biophys Acta 2011;1808(8):2045–2050.
830 [93] Chung MT, Levi B, Hyun JS, et al. Pierre Robin sequence and Treacher Collins
831 hypoplastic mandible comparison using three-dimensional morphometric analysis. J
832 Craniofac Surg. 2012;23(7 Suppl 1):1959-1963. doi:10.1097/SCS.0b013e318258bcf1.
833 [94] McDonald MT, Gorski JL. Nager acrofacial dysostosis. J. Med. Genet. 1993; 30:779–
834 782.
835 [95] Sperber, G. H., Sperber, G. H., Guttmann, G. D., Sperber, S. M., & Gutterman, G. D.
836 (2001). Craniofacial development. PMPH-USA.
837
838
839
840

Author contributions

Dr. Anne Morice contributed to the conception, design, acquisition, analysis, and interpretation of the data, writing and revision of the manuscript.

Dr. Raphael Cornette contributed to the acquisition and analyses of the data and critical analysis of the manuscript.

Dr Amerigo Giudice contributed to the acquisition of the imaging data.

Dr Corinne Collet contributed to the acquisition of the genetic diagnoses.

Drs Eric Arnaud, Giovanna Paternoster, Eva Galliani and Pr Arnaud Picard contributed to the selection of the cohort and management of the patients.

Drs Laurence Legeai-Mallet and Roman Hossein Khonsari contributed to the conception, design, analysis, and interpretation of the data and the critical analysis of the manuscript.

All of the authors contributed to the revision of the manuscript and approved the final version.

Funding sources statement: This research did not receive any specific grant from funding agencies in the public, commercial, or not-for-profit sectors.

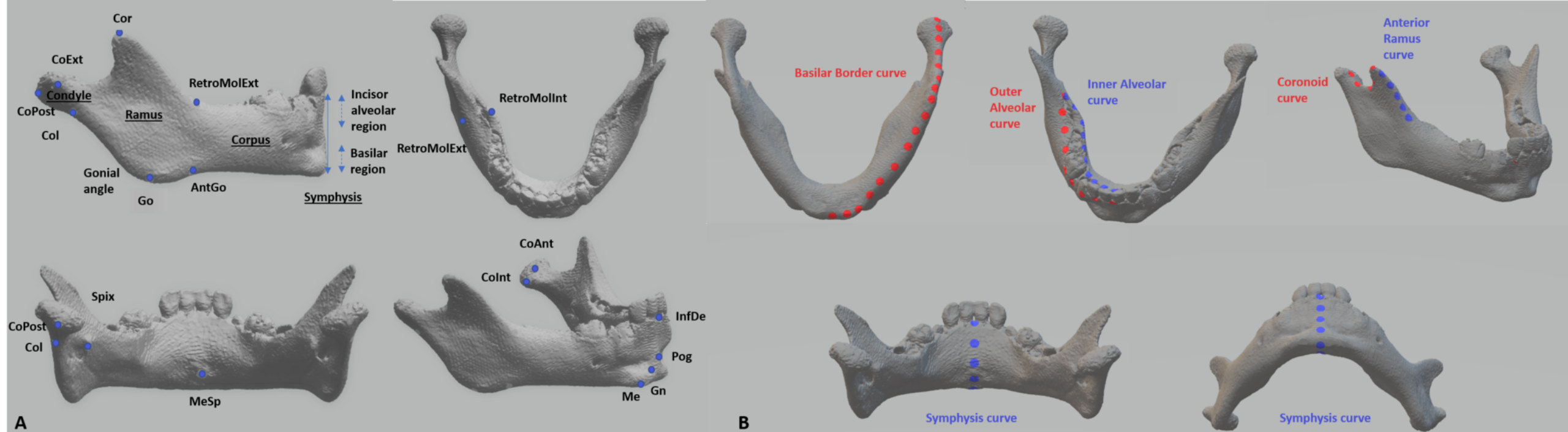
Cor
CoExt
Condyle
CoPost
Col
Ramus
RetroMolExt
Corpus
Gonial angle
Go
AntGo
Incisor alveolar region
Basilar region
Symphysis
RetroMolInt
RetroMolExt
Spix
CoPost
Col
MeSp
CoAnt
CoInt
InfDe
Pog
Gn
Me
A
Basilar Border curve
Outer Alveolar curve
Inner Alveolar curve
Coronoid curve
Anterior Ramus curve
Symphysis curve
Symphysis curve
B

A

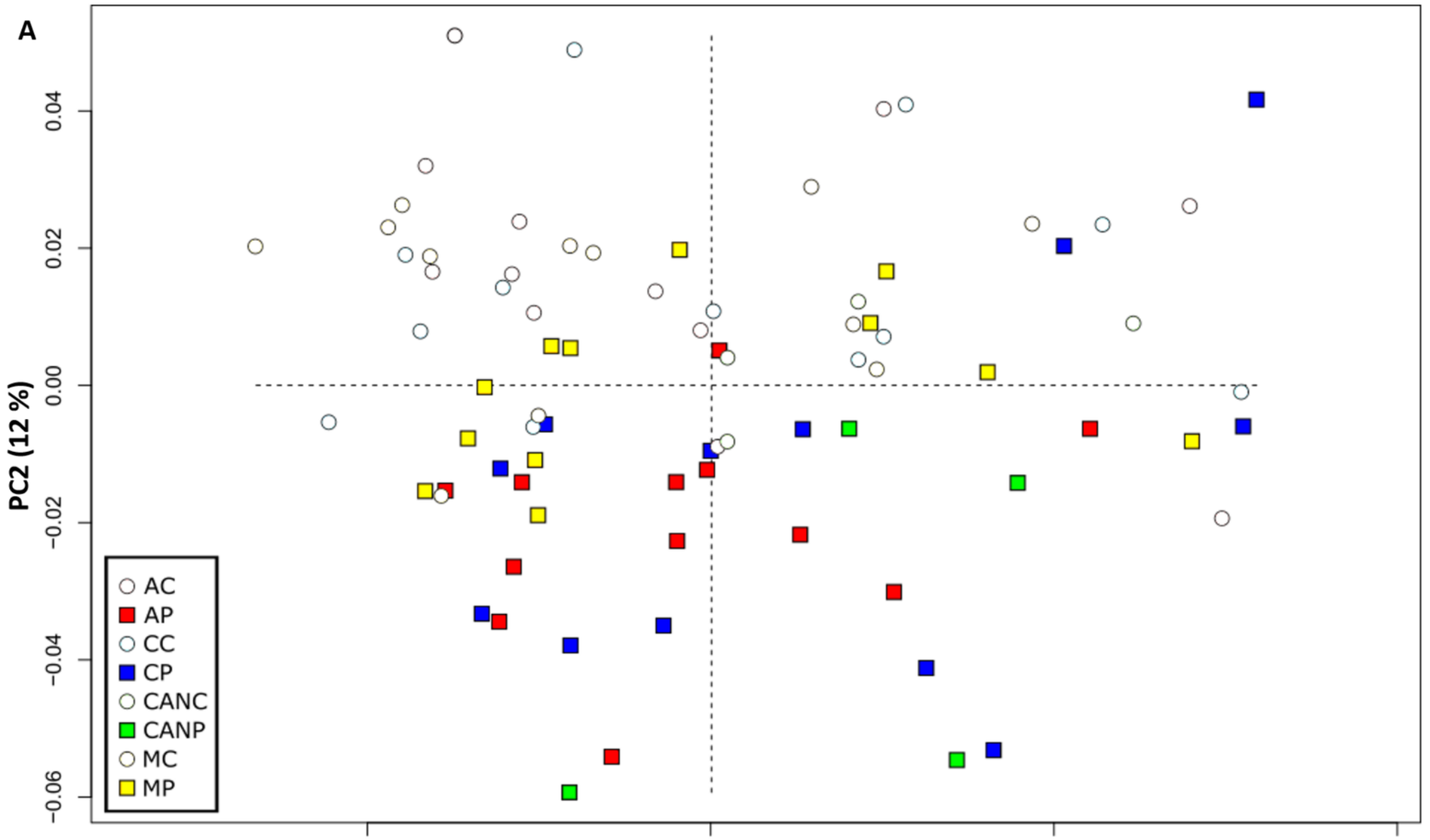
PC2 (12 %)
0.04
0.02
0.00
−0.02
−0.04
−0.06
AC
AP
CC
CP
CANC
CANP
MC
MP
−0.05
0.00
0.05
0.10
PC1 (28.5 %)

B

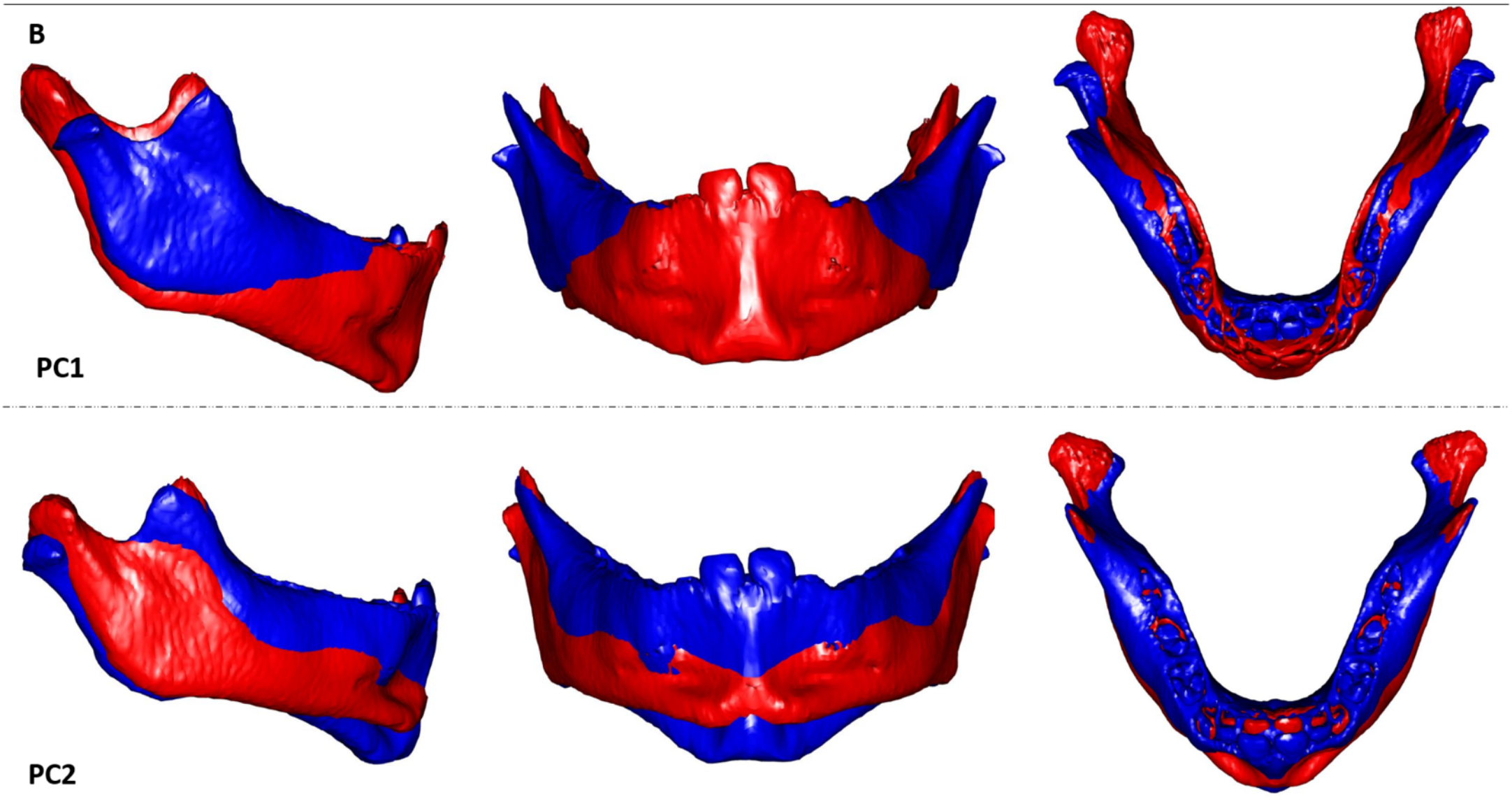
PC1
PC2

A

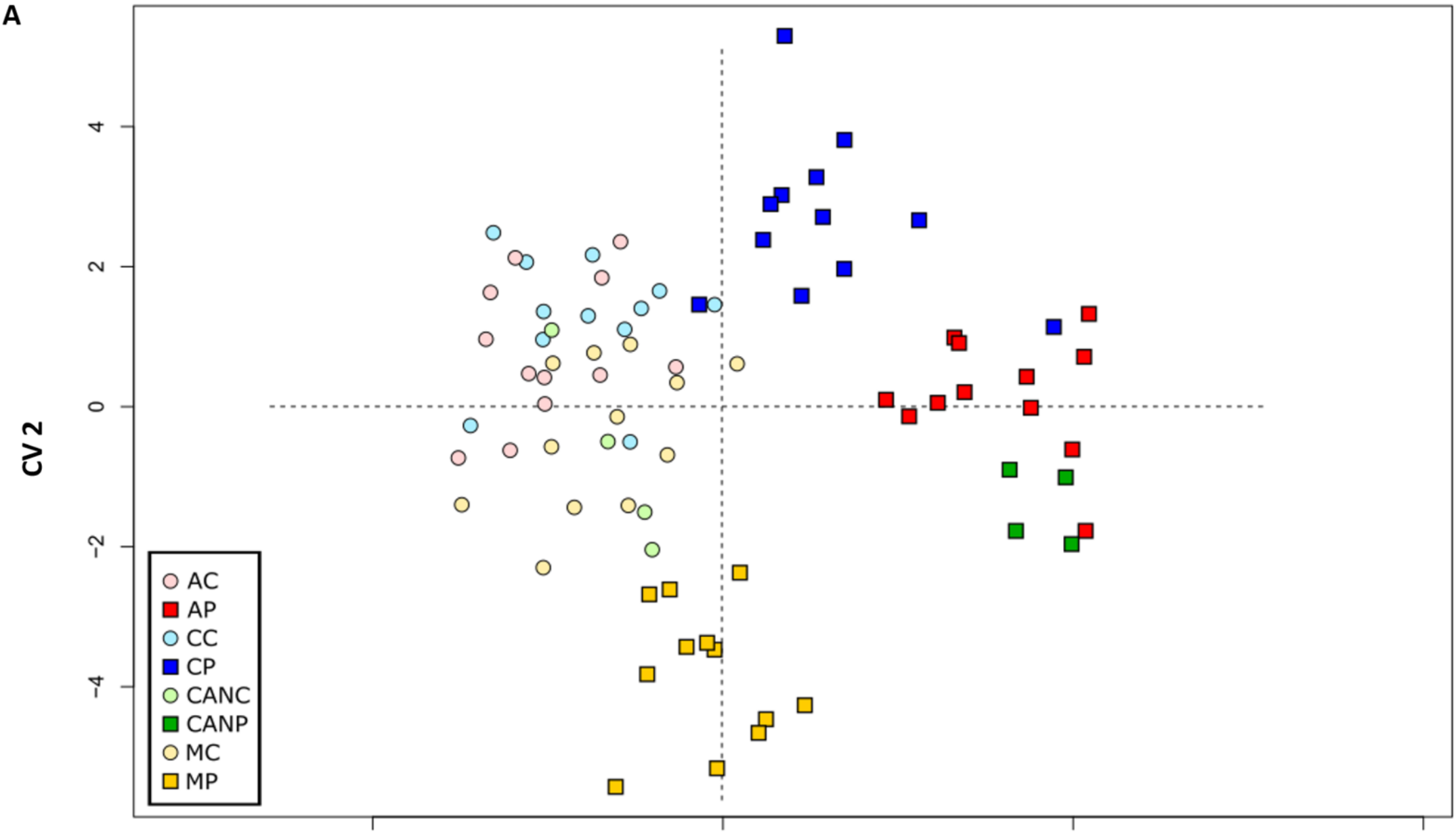

B

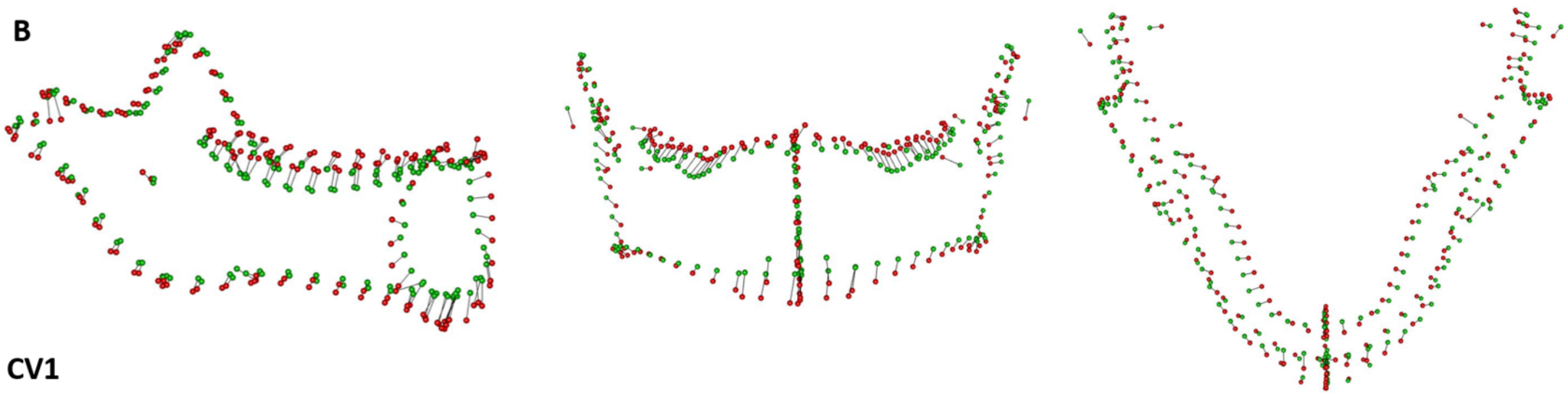

A: Crouzon vs controls

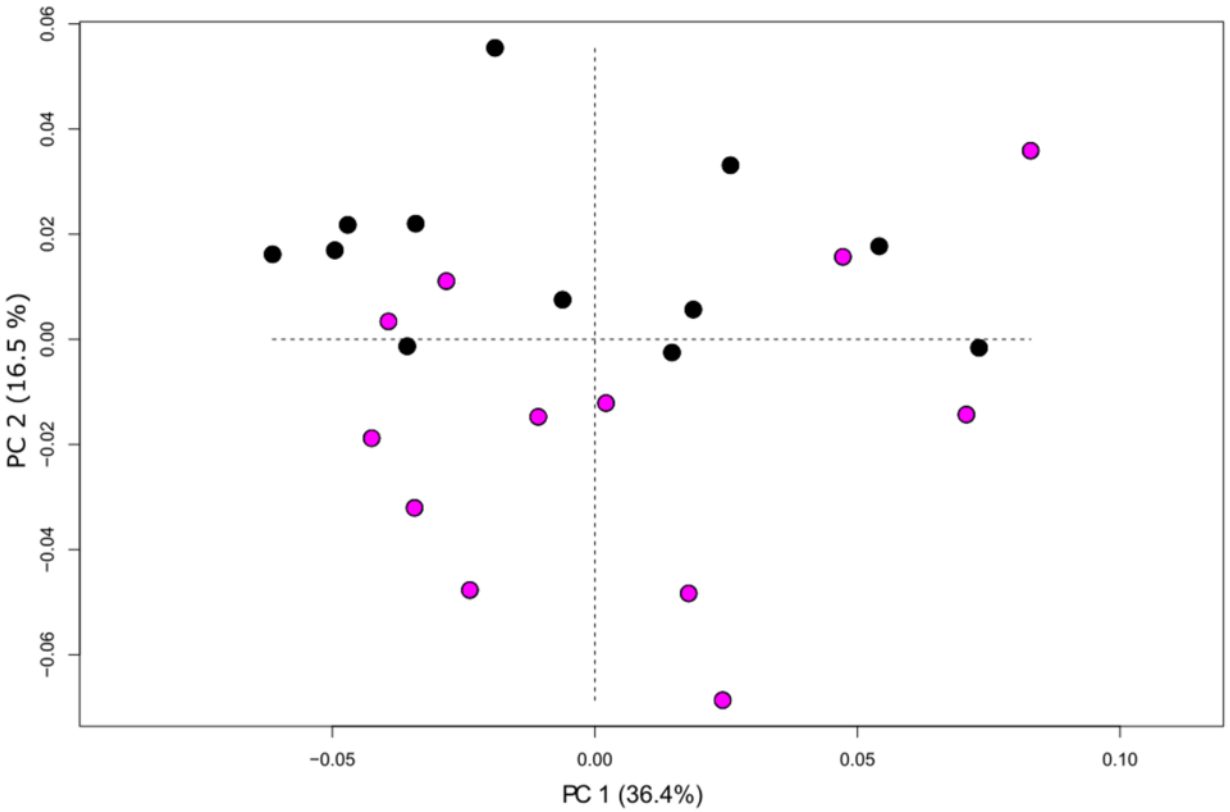

B: Apert vs controls

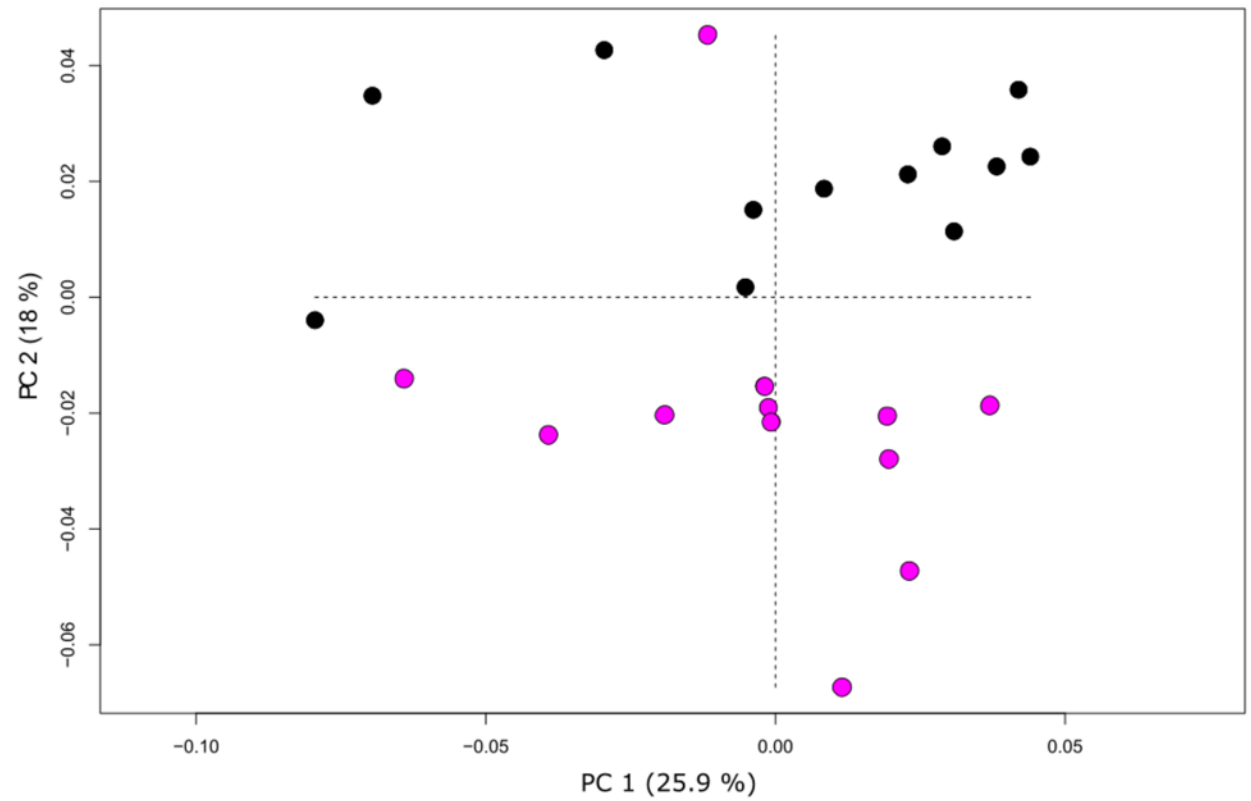

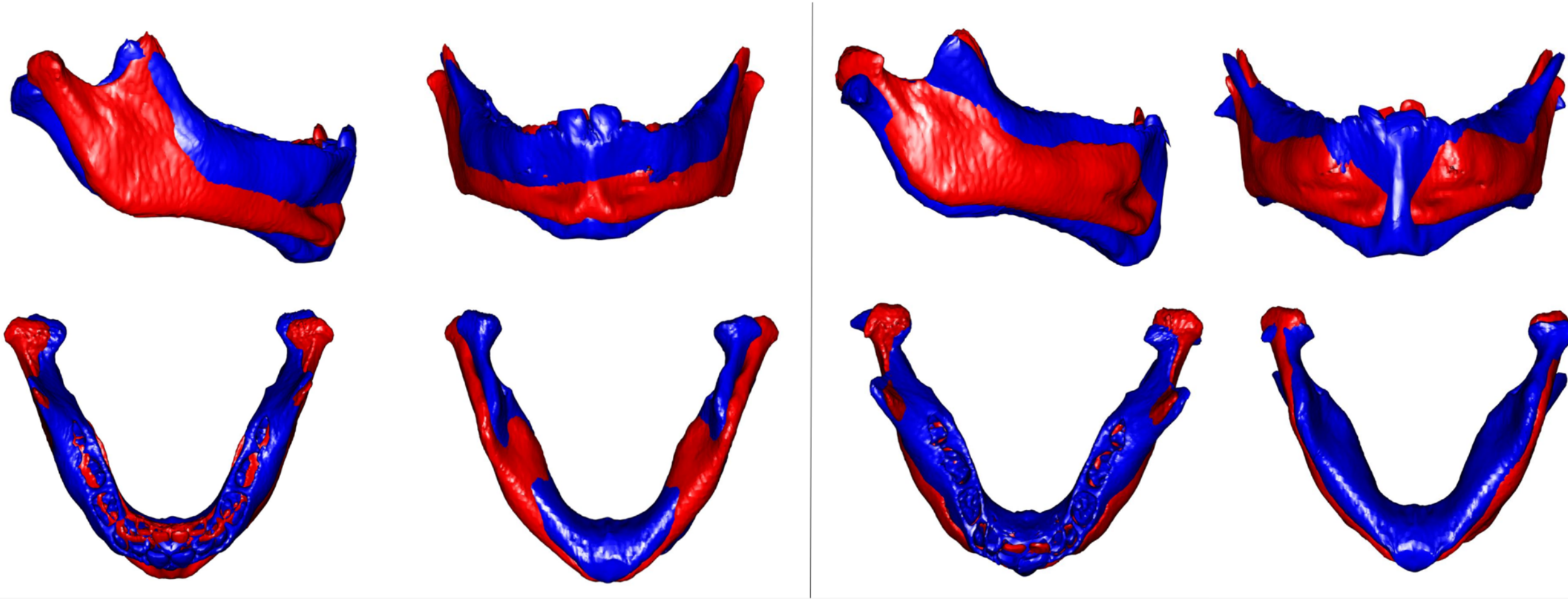

A: Muenke vs controls

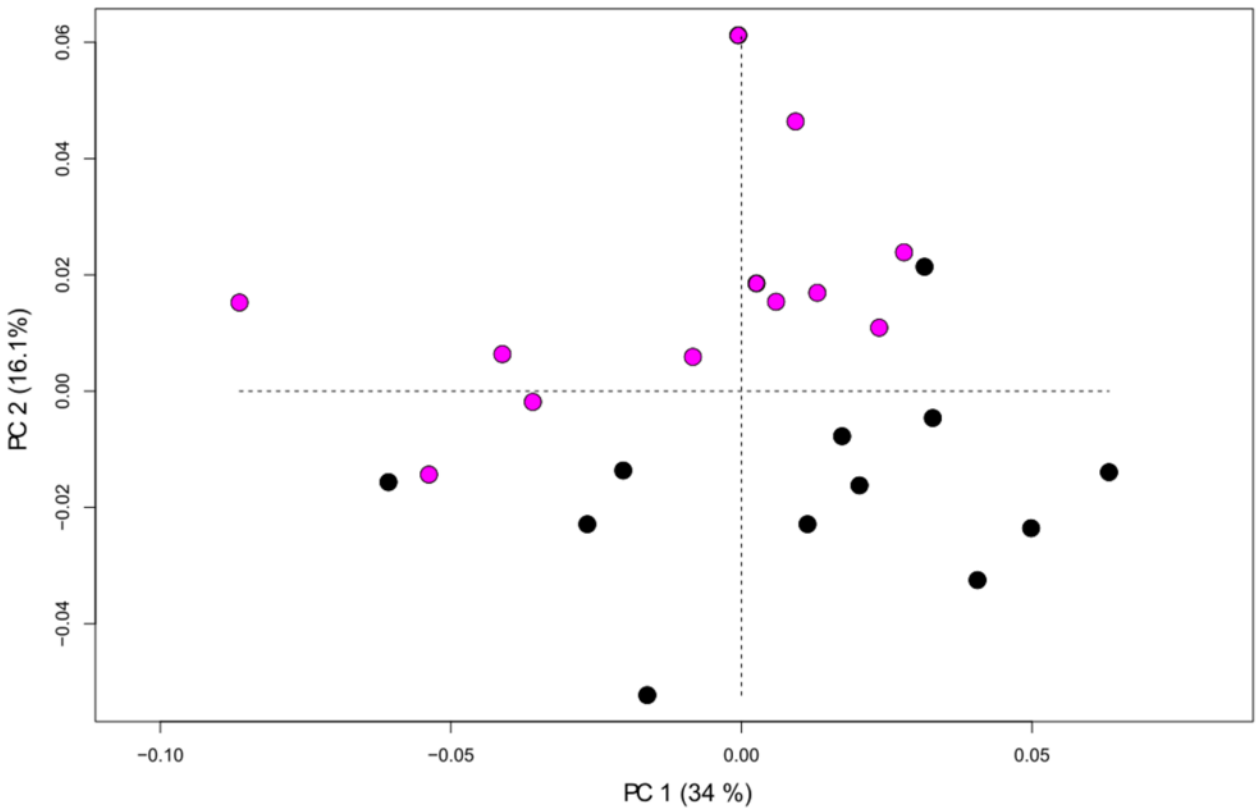

B: CAN vs controls

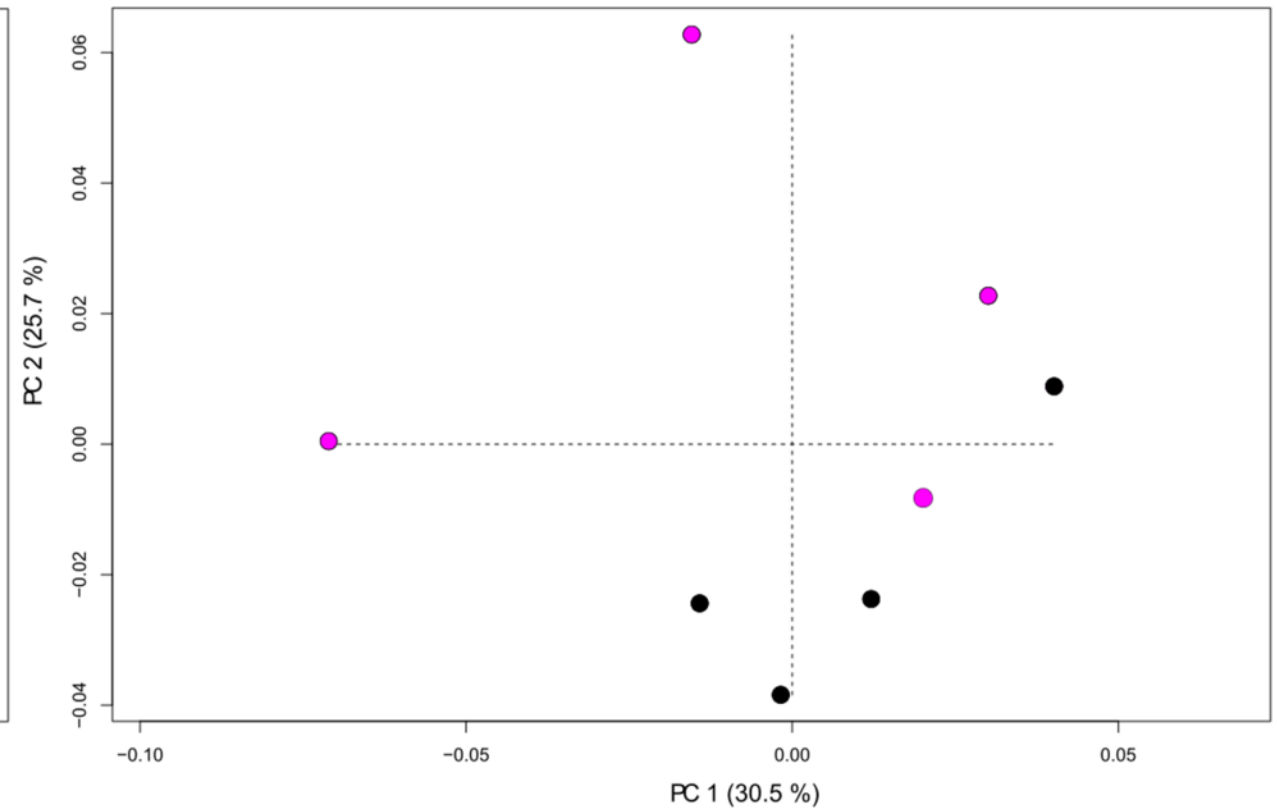

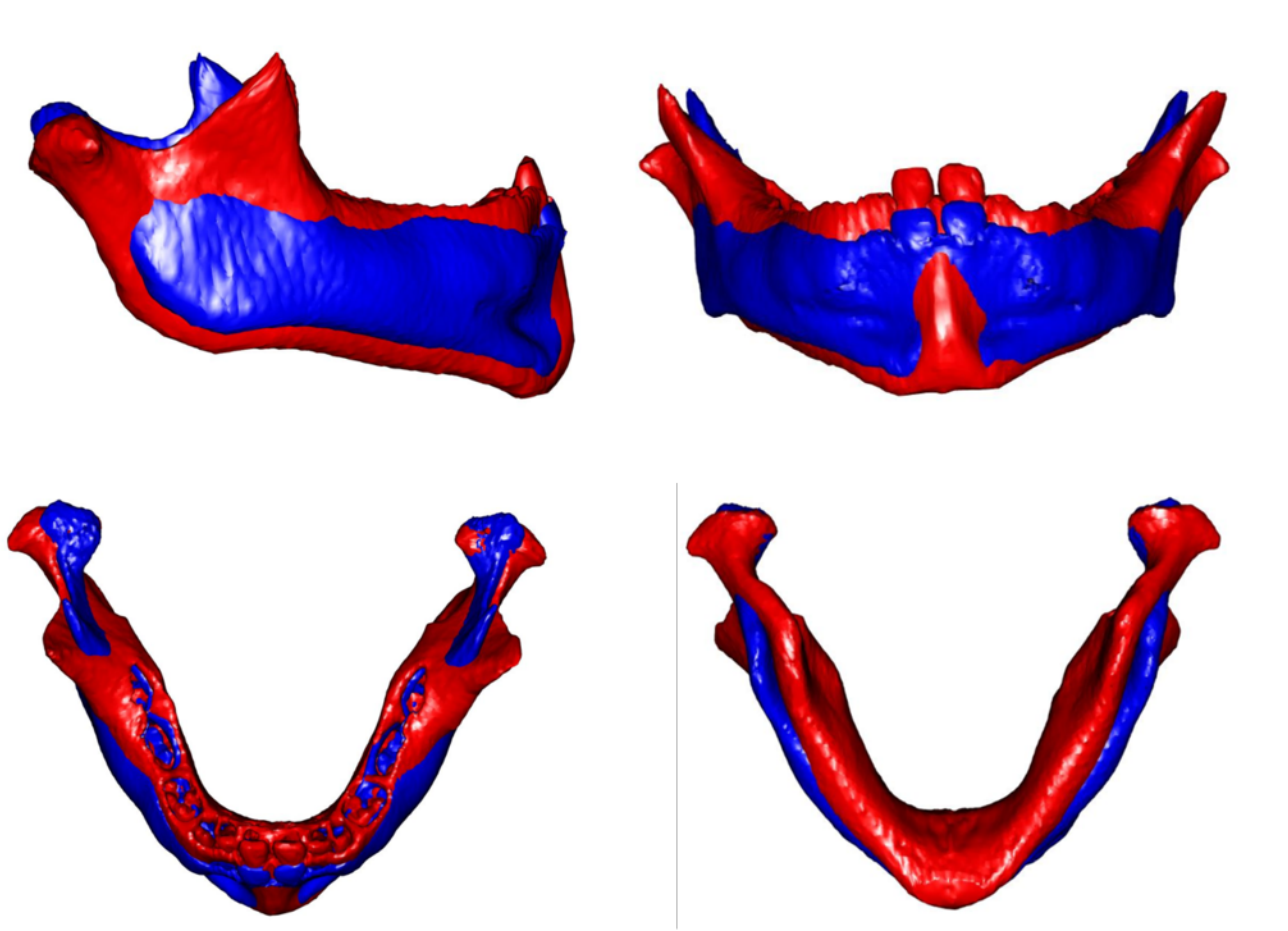

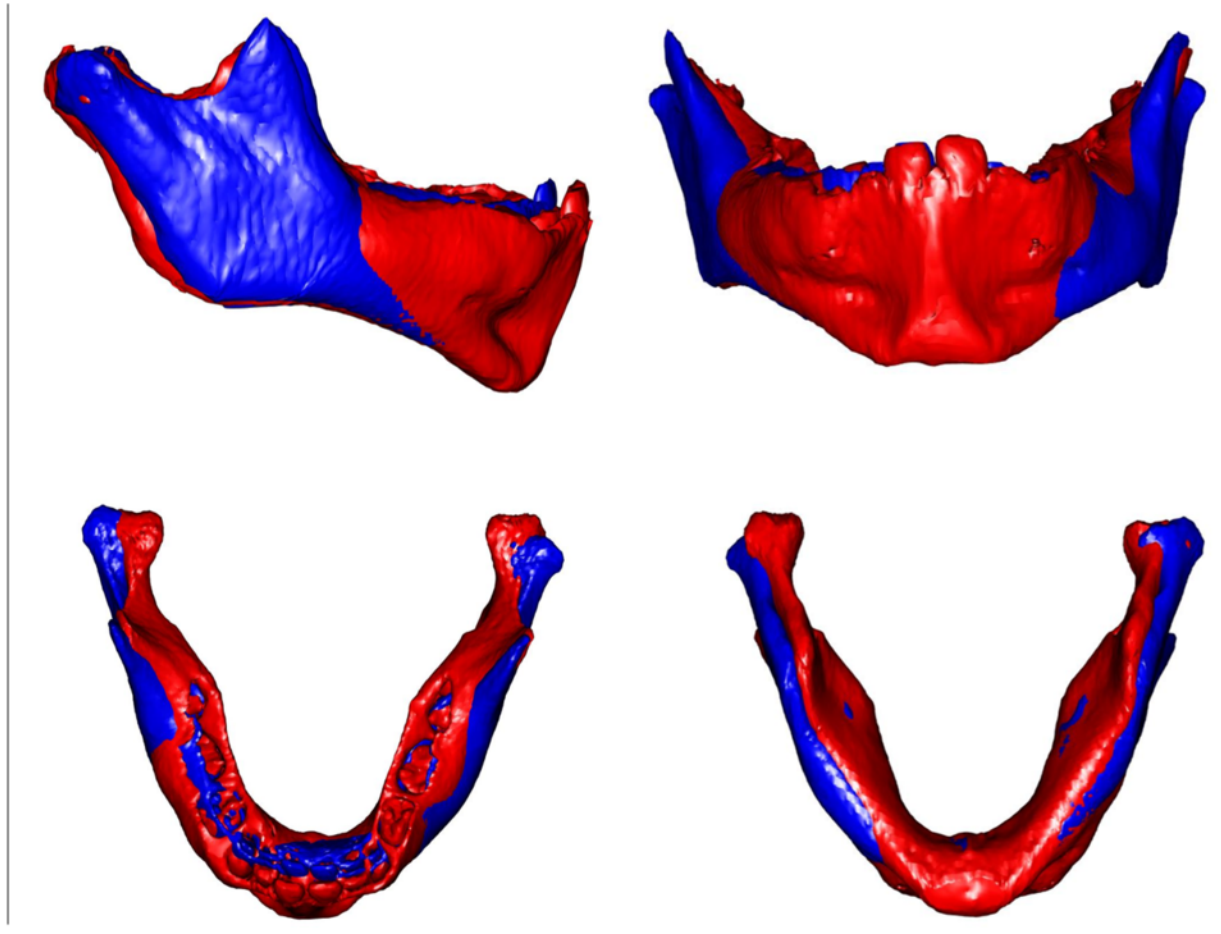

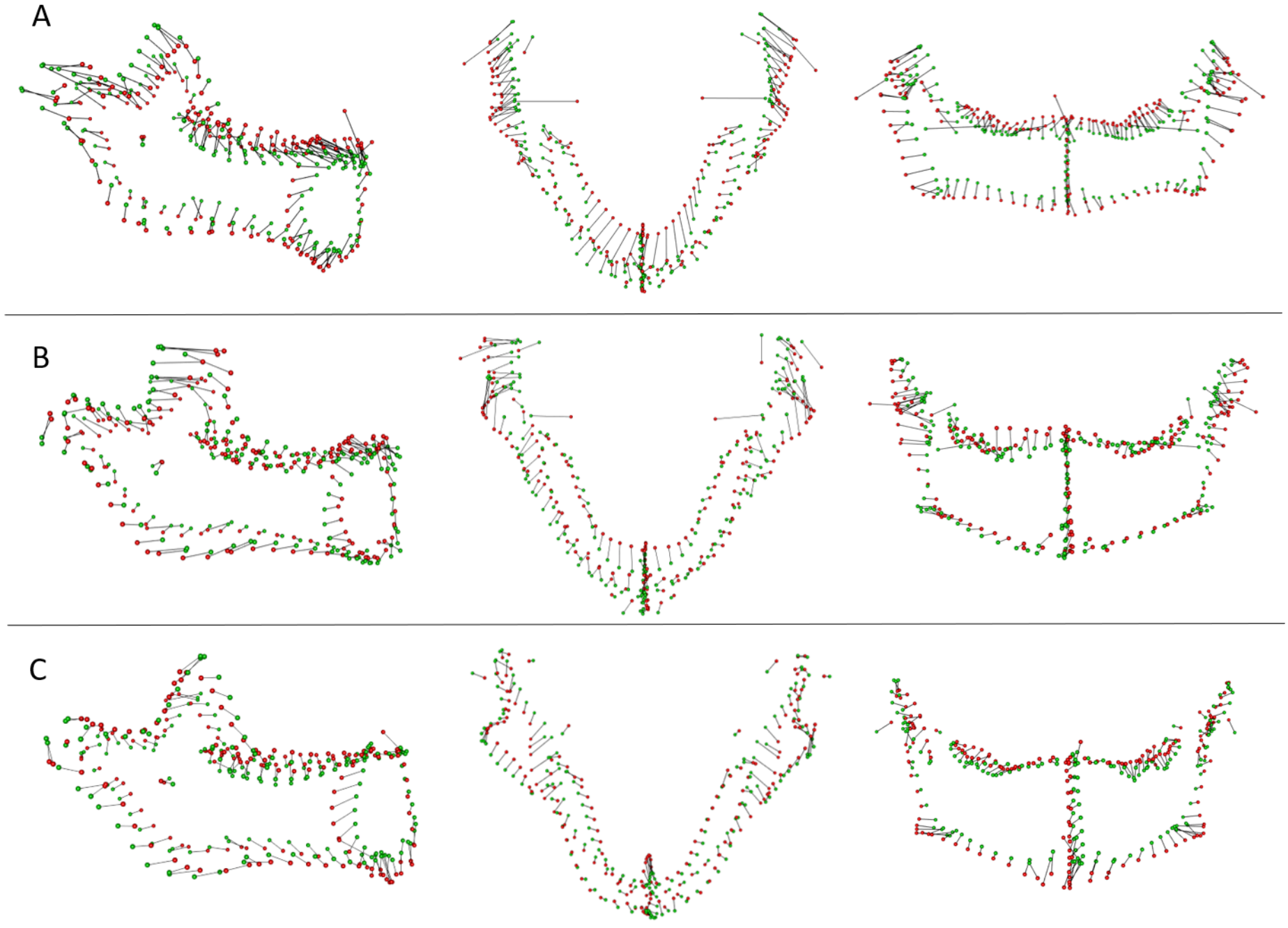
A
B
C